Applying a [^{11}C]Raclopride Template to Automated Binding Potential Estimation in HRRT Brain PET

Philip Novosad, Marie Bieth, Paul Gravel, Herve Lombaert, Kaleem Siddiqi, Andrew J. Reader

***Abstract*–Performing kinetic analysis of [^{11}C]raclopride PET data typically involves user intervention to identify key volumes of interest, such as the cerebellum for the reference region and the caudate and putamen for regions where the binding potential (BP) needs to be estimated. In many PET centres, this process is neither automated nor standardized, possibly producing discrepancies between centres. Conventionally, MR anatomical images are used to identify the key volumes of interest, but this is difficult to automate robustly, and user intervention can sometimes be required. This work considers instead the use of an anatomically labeled [^{11}C]raclopride template, formed from multiple subjects, which has the key advantages of low noise, good resolution and having a highly similar spatiotemporal intensity distribution to any given single subject raclopride scan. This makes the template an excellent target for automated image registration and segmentation. We present a methodology which works on post-reconstruction images, demonstrating an automated and consistent way of identifying key regions of interest (ROIs) and determining binding potential without any MR image or user intervention. The performance of the methodology is evaluated using simulated and real [^{11}C]raclopride data. The simplified reference tissue model with the basis function method (SRTM-BFM) was used for the kinetic modeling.**

I. Introduction

CONVENTIONAL identification of ROIs in brain PET images is accomplished manually or by registration to MR images. Manual techniques are prone to subjective bias on the part of the user, introducing inter- and intra-user discrepancies, and are both time-consuming and challenging because of the inherent noise in PET images. In addition, registration of PET images to MR images is not optimal because the two modalities may have different resolution, different relationships between relative intensity and anatomy, and may suffer from different image artifacts. Moreover, exploiting anatomical information is not necessarily pertinent, because the distribution of receptor density can be heterogeneous within brain structures.

This work considers the use of an average-shape and average-intensity anatomically labeled radioligand-specific template for automatic segmentation of key ROIs used in PET kinetic analysis. In contrast to MR anatomical images, a radioligand-specific PET template is very similar in its spatiotemporal intensity, and registration of single subject data to the template is straightforward. We evaluate the methodology for the case of real and simulated [^{11}C]raclopride data for the high resolution research tomograph (HRRT) [1].

P. Novosad, P.Gravel and A.J. Reader are with the Montreal Neurological Institute, McGill University, Montreal, Canada.

M. Bieth, H. Lombaert and K. Siddiqi are with the School of Computer Science and the Center for Intelligent Machines, McGill University, Montreal, Canada.

II. Overview of Methodology

The general strategy developed in this paper draws on previous work using MR templates to segment brain volumes [2]. Given an anatomically labeled brain volume (template) and a subject brain volume, the propagation of anatomically labeled voxels from the template to the brain volume can be thought of as a registration problem. In order to segment the brain volume, the non-linear transformation that best maps the spatial intensity distribution from the subject brain volume to the template must be computed. Applying the inverse transform to the anatomically labeled voxel dataset propagates the labels to the subject brain volume and completes the segmentation.

In this work, a high quality anatomically labeled radioligand-specific PET template is targeted in the intensity-based registration for segmentation. The template has two key characteristics that make it a well suited registration target: average-shape and average-intensity. In addition, the high signal-to-noise ratio makes it an optimal image choice for manually labeling anatomical ROIs for segmentation.

Subsequently, regional BP estimation on the segmented subject brain volume is done. The time-activity curves (TACs) of each voxel in the identified regions are averaged to obtain regional TACs which are fitted with a kinetic model.

III. Methods

Segmentation of a brain volume using this methodology depends on a two-part design for the template [2]. The template contains not only a high quality average shape and intensity volume, but also a set of labels defined on the average brain volume. To segment a given time-summed subject, it is registered to the average time-summed brain volume to obtain a forward transformation. The forward transformation is then inverted and applied to the labels defined on the average brain, propagating the labels to the subject brain. Note that any labeled set of voxels can be defined on the average brain volume to be used for segmentation, and that the transformation itself is only dependent on the average brain volume and not the overlaid set of labels.

A. *Image Registration*

Registration of the time-summed average brain volume and the time-summed subject brain volume was accomplished in two steps. The first step accounts for the linear component of the transformation using a 12-parameter (3 scales, 3 shears, 3 translations and 3 rotations) affine transformation. The second step accounts for morphological differences in the anatomy between the subject brain volume and the average brain volume. A non-linear diffeomorphic log-demons registration was used for this purpose. The diffeomorphic log-demons algorithm (DLD) was proposed by *Vercauteren et al.* [3], and uses the Lie group structure that defines an exponential mapping from the vector space of smooth stationary velocity fields to diffeomorphisms. The objective function to minimize is:

$$E(s,c)=\frac{1}{\sigma_i^2}Dis(F,M,c)+\frac{1}{\sigma_x^2}dist(s,c)^2+\frac{1}{\sigma_T^2}Reg(s) \quad (1)$$

where F the fixed image, M the moving image, c the current non-regularized transformation and s is the regularized transformation, which can be understood as the exponential of a stationary velocity field v. The first term is the dissimilarity between the transformed moving image and the fixed image. The second term is the distance between the regularized and non-regularized transformation, and the last term is the regularization term. We classically have $Dis(F,M,c) = \|F - M \circ c\|^2$, $Reg(s) = \|\nabla s\|^2$ and $dist(s,c) = \|s - c\|$. The optimization of the energy is implemented with two consecutive smoothing steps which use two parameters, both being widths of Gaussian kernels: K_{fluid} controls smoothing of the update field and has a fluid behavior, and K_{diff} controls smoothing of the displacement field and has an elastic behavior.

For our experiments, we chose $K_{fluid} = 0.5$, $K_{diff} = 1.5$ and $\sigma_i = \sigma_x = 1$ empirically. The choice of the registration parameters is a difficult and task-dependent problem. See [3] for more details.

B. *Atlas Construction*

Average shape and intensity brain volumes were constructed using the methodology described by Lombaert *et al* [4]. For a set of *N+1* subject brain volumes in the affine space of the reference volume, the procedure for building the average morphological brain volume R', using the DLD algorithm, is summarized in (1) below:

$$R' = \left[\frac{1}{N}\sum_{i=1\dots N} I_i \circ \exp(v_i)\right] \circ \exp\left(-\frac{1}{N}\sum_{i=1\dots N} v_i\right) \quad (2)$$

where v_i is the stationary velocity field of the warping from I_i to the current reference volume. Explicitly, for a set of N subject brain volumes in the affine space of the reference brain volume, a non-linear transformation between each subject brain volume and the reference brain volume is performed. The non-linearly registered subject volumes are then intensity-averaged, and the transformation updating the reference image is computed (in the log-domain using the negated stationary velocity fields) and applied. The initial reference is an arbitrary subject brain volume in the set, and is independent of the choice of the reference volume. This process can be repeated using the resulting average-shape and average-intensity volume as the reference for the next iteration, the effect of which is to reduce the average distance from each subject volume in the set to the average volume.

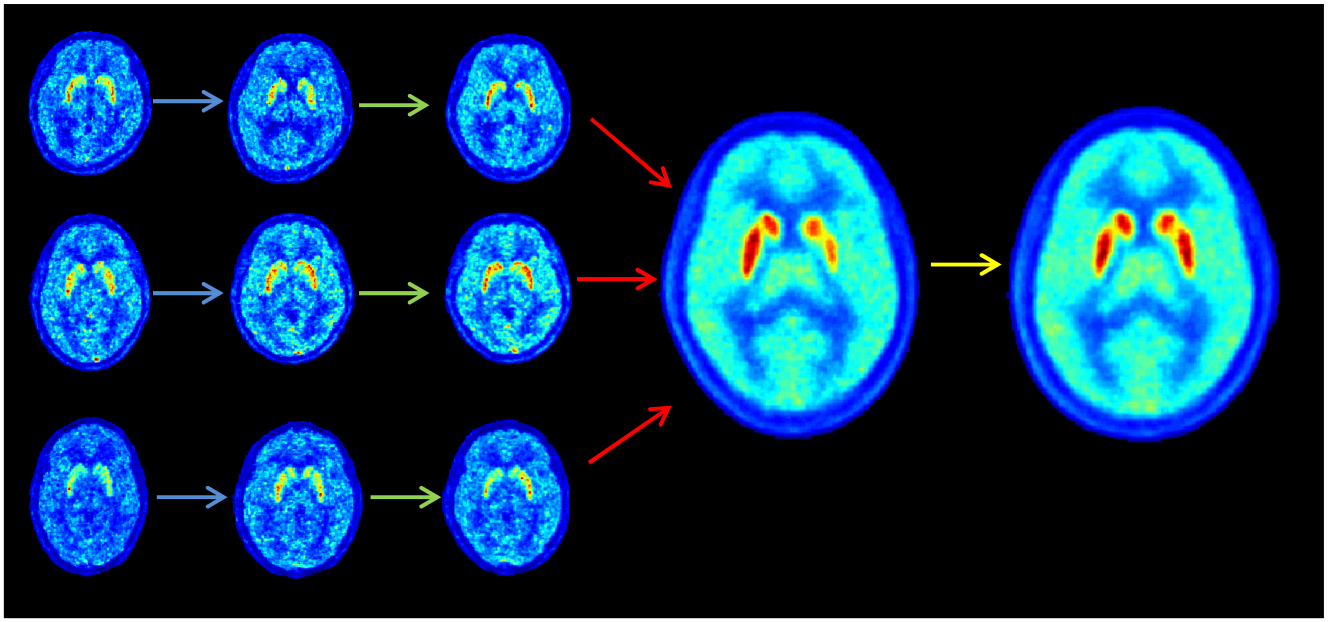

Fig. 1: Average brain volume construction from real HRRT [^{11}C]raclopride subjects. Each subject brain volume is linearly registered to an arbitrary reference image (blue arrow). The linearly registered volumes are again each registered with the DLD algorithm to the reference volume (green arrow) and then intensity averaged (red arrow). Finally, the transformation updating the reference image is computed and applied as in (2) (yellow arrow).

The method is evaluated using a realistic [^{11}C]raclopride phantom and real [^{11}C]raclopride HRRT PET scans of 16 healthy volunteers.

A. [^{11}C]Raclopride Phantom Study

1) Generating Simulated Data: simulated evaluation of the methodology employed a modified numerical phantom from Rahmim *et al* [5]. It is a 256×256×207 3D image containing seven defined ROIs: grey matter, white matter, the cerebellum, the left and right caudate and the left and right putamen. 16 different dynamic phantoms were generated, each with 26 time frames (frame length: 6×30s, 7×60s, 5×120s and 8×300s). A realistic and unique set of TACs was incorporated into each of 16 dynamic phantoms by assigning each region of each frame a count value based on TACs derived from [^{11}C]raclopride scans of healthy subjects at the Brain Imaging Center (BIC) of the Montreal Neurological Institute (MNI). To simulate the real variation in brain anatomy between subjects, each of the 16 brain phantoms was non-linearly registered to different static reconstructions of real 60 minute [^{11}C]raclopride scans using the DLD algorithm. The simulated data were reconstructed using the standard procedure of 10 iterations of the Ordinary Poisson Ordered Subset Expectation Maximization algorithm (OP-OSEM) with 16 subsets [6]-[8]. Resolution modeling was included in the reconstruction [9]-[10]. However, the noise level in the simulations is still lower than that encountered in reality due to the effects of scatter, randoms and detector dead time. See Fig. 2.

The non-linearly registered dynamic phantoms were forward projected into 2209 sinograms (each of 256×288 bins), and noise was introduced in each realization by drawing counts from the Poisson distribution with the mean as the count value in the sinogram bin. The sum of sinogram counts was chosen to be the same as a typical one hour 370 MBq [^{11}C]raclopride scan on the HRRT. Attenuation effects were simulated. One noisy reconstruction was generated for each of 15 anatomically unique numerical phantoms using 10 iterations of OP-OSEM with 16 subsets. An average shape and intensity volume was constructed from the 15 noisy reconstructed phantom brain volumes, and 5 ROIs were manually labeled (the cerebellum, left and right putamen and left and right caudate) as shown in Fig. 3.

2) Simulated Evaluation: The methodology was assessed on the ability to recover the true BP of a simulated test subject. Thirty noisy realizations of a single anatomically unique dynamic phantom were generated. For each of 30 noisy realizations of the same test subject, the anatomical labels defined on the simulated average image volume were mapped through a transformation to segment the 5 regions on the noisy test subject volume (Fig. 3). The segmented regions were used to compute average regional TACs which were fitted using SRTM-BFM (100 basis functions, θ_3 ranging from 0.001 s^{-1} to 0.01 s^{-1}). We compared the BP obtained by fitting the average regional TACs, obtained from the segmented regions, to the BP obtained by fitting the average regional TACs, obtained from the true regions. Therefore we are comparing the BP using our methodology to the BP that would be obtained if we had perfect knowledge of the true ROIs. See Fig. 4. We investigated the accuracy of the template based segmentation by comparing the segmented regional volumes to the true regional volumes defined on the test subject. We used three measures for the comparison: the Dice similarity coefficient (DSC), the percent difference between regional TACs and the percent difference between regional BPs:

$$DSC = 2 \times \frac{V_{TEMPLATE} \bigcap V_{TRUE}}{V_{TEMPLATE} + V_{TRUE}} \quad (3)$$

$$\kappa = \frac{1}{T}\sum_{t=1}^{T}\left(\frac{TAC_{TEMPLATE}(t) - TAC_{TRUE}(t)}{TAC_{TRUE}(t)}\right) \times 100\% \quad (4)$$

$$\alpha = \frac{BP_{TEMPLATE} - BP_{TRUE}}{BP_{TRUE}} \times 100\% \quad (5)$$

where $\bigcap$ denotes the intersection operation, $V_{TEMPLATE}$ is the volume of a segmented region, and V_{TRUE} is the true region as defined on the test volume. In equation (4), the TAC for a particular segmented region was obtained by averaging the TACs of each voxel in that region; in equation (5) the BP was obtained by fitting the regional TAC. The simulated results are summarized in Table I. It is evident that including the non-linear registration significantly improves segmentation results.

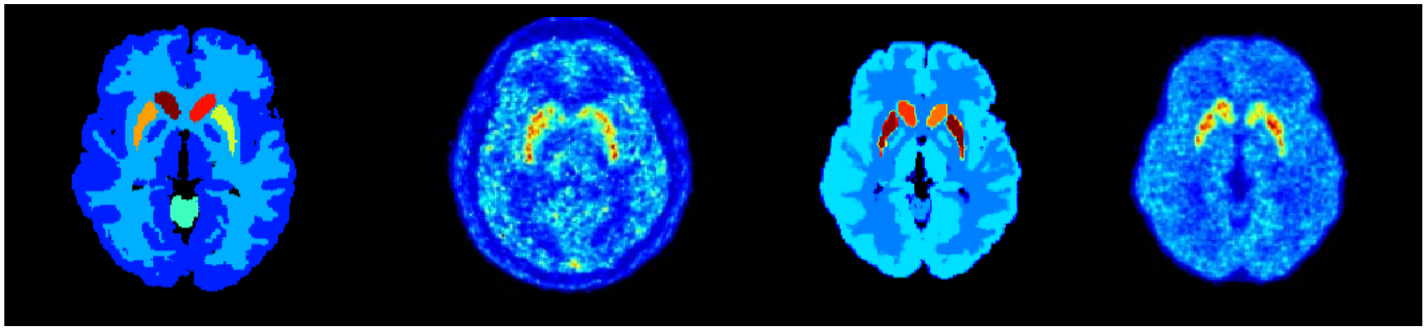

Fig. 2: Generation of a simulated subject. Left to right: numerical phantom, real HRRT registration target, warped dynamic phantom, reconstructed phantom.

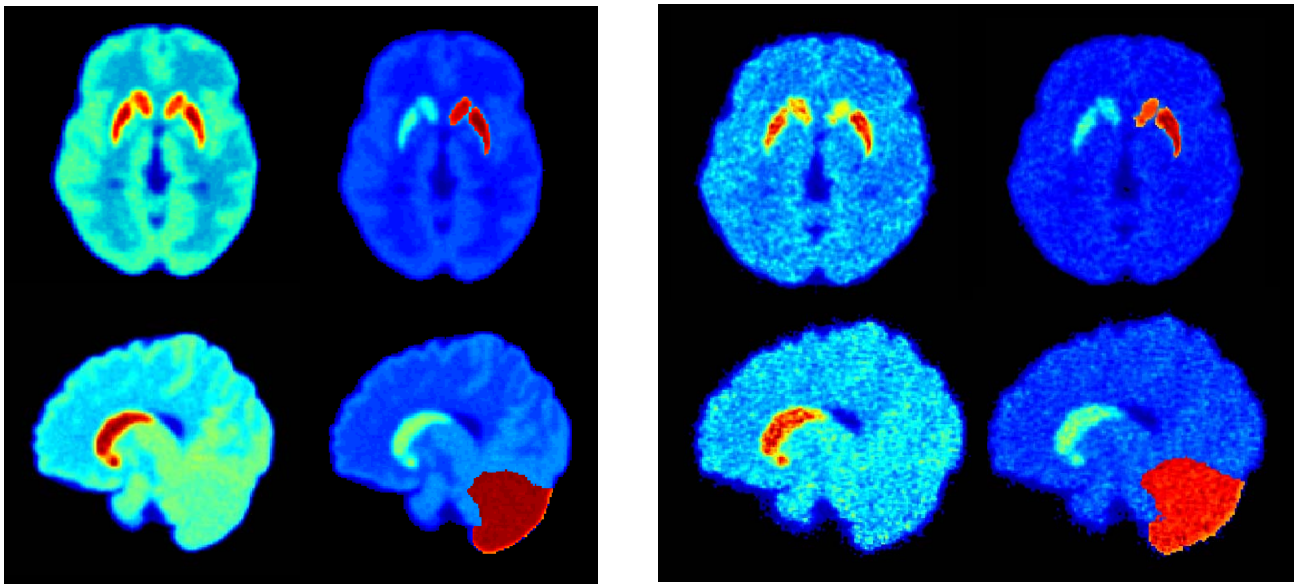

Fig. 3. Left: average brain volume built from 15 anatomically unique noisy reconstructions of the dynamic phantom with manually defined labels superimposed on average brain volume. Right: noisy realization of simulated test subject, showing template-based segmentation of putamen, caudate and cerebellum.

TABLE I: SIMULATED VALIDATION OF PET TEMPLATE BASED SEGMENTATION

	$\overline{DSC}$	$\overline{\alpha}$ (%)	$\overline{\kappa}$ (%)
	Affine Registration Followed By DLD Registration		
Left Putamen	$0.89 \pm (0.02\times10^{-2})$	0.27 ± 0.66	0.40 ± 0.30
Right Putamen	$0.86 \pm (0.05\times10^{-2})$	-2.38 ± 0.60	-1.03 ± 0.41
Left Caudate	$0.89 \pm (0.02\times10^{-2})$	1.17 ± 0.62	1.74 ± 0.32
Right Caudate	$0.89 \pm (0.03\times10^{-2})$	-1.11 ± 0.71	-1.72 ± 0.45
Cerebellum	$0.95 \pm (0.07\times10^{-3})$	---	0.41 ± 0.08
	Affine Registration Only		
Left Putamen	$0.71 \pm (0.01\times10^{-1})$	-8.29 ± 2.34	-4.01 ± 0.86
Right Putamen	$0.77 \pm (0.01\times10^{-1})$	-2.73 ± 2.68	0.65 ± 0.91
Left Caudate	$0.74 \pm (0.02\times10^{-1})$	-15.61 ± 3.56	-10.14 ± 1.62
Right Caudate	$0.80 \pm (0.02\times10^{-1})$	-4.74 ± 3.47	-3.14 ± 1.46
Cerebellum	$0.94 \pm (0.07\times10^{-2})$	---	0.61 ± 0.97

All values shown as mean plus or minus one standard deviation.

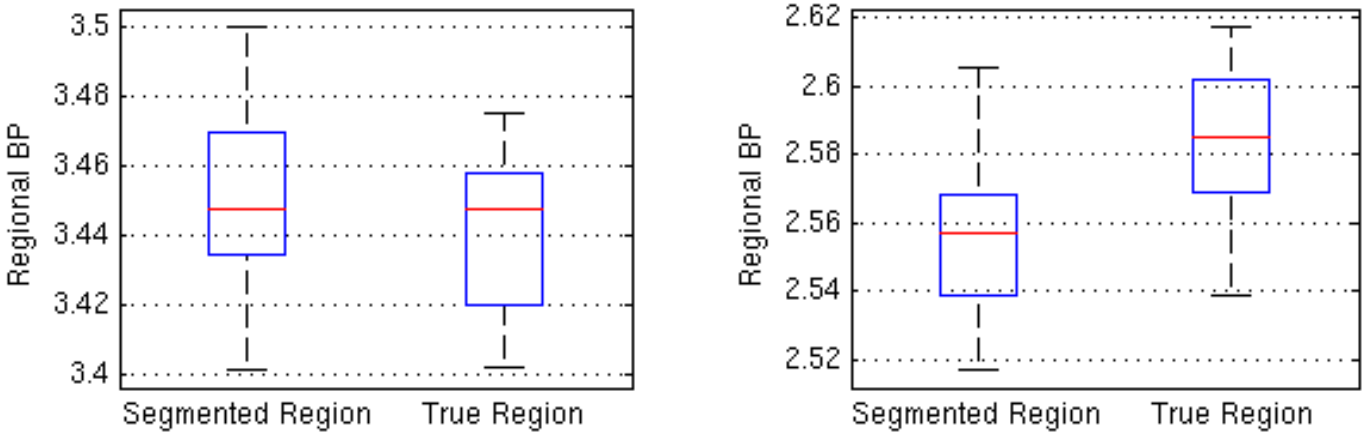

Fig. 4: Distribution of regional BP values across 30 noisy realizations of a simulated test subject, using segmented and true regions for kinetic analysis. Left: distribution of regional BP for the left putamen. Right: distribution of regional BP for left caudate. Registration to obtain the segmented regions was done with affine followed by DLD. Registration to obtain the segmented regions was done with affine followed by DLD. The red line represents the median value of each distribution. The edges of the box are the 25th and 75th percentiles, and the whiskers extend to the most extreme data points.

B. *Real HRRT [^{11}C]Raclopride Study*

Sixteen real [^{11}C]raclopride scans of healthy subjects, acquired at the BIC of the MNI were used to generate an average shape and average intensity template (Fig. 5). The scans were 60 minutes long, the size of the 4D images are 256×256×207×26 voxels, and each voxel is 1.22×1.22×1.22 mm^3 in size. The scans were reconstructed using 10 iterations of OP-OSEM with 16 subsets. Five ROIs were manually identified on the average image (cerebellum, left putamen and caudate, right putamen and caudate).

The PET template based segmentation method was compared to a standard MR registration based segmentation method (CIVET [12]-[17]). Using CIVET, the volumes corresponding to five regions of interest (cerebellum, left and right caudate, left and right putamen) for each of 15 [^{11}C]raclopride scans with accompanying MR anatomical images were automatically identified. The segmented ROIs were compared in terms of the Dice similarity coefficient:

$$DSC_{DIFF} = 2 \times \frac{V_{MR} \bigcap V_{PET}}{V_{MR} + V_{PET}} \quad (6)$$

where V_{MR} is the volume of the structure as identified using CIVET and V_{PET} is the volume of the structure as identified using our method. See Fig. 6 and 7.

Another meaningful comparison between the two methods is that of the extracted regional TACs and regional BP estimation. We estimated regional BP using the segmented volumes obtained with CIVET by averaging each voxel in the region and fitting the average TAC using the SRTM-BFM (100 basis functions, θ_3 ranging from 0.001 s^{-1} to 0.01 s^{-1}) and compared the results to the regional BP values calculated from our method.

The percentage difference between the BP estimations for a particular region in a given scan is defined as:

$$\alpha_{DIFF} = \frac{BP_{PET} - BP_{MR}}{BP_{MR}} \times 100\% \quad (7)$$

where BP_{MR} is the regional BP for a particular region using the CIVET derived volumes, and BP_{PET} is the regional BP of for the same region using volumes derived from the template. The percentage difference between the TACs extracted for a particular region in a given scan is defined as:

$$\kappa_{DIFF} = \frac{1}{T}\sum_{t=1}^{T}\left(\frac{TAC_{PET}(t) - TAC_{MR}(t)}{TAC_{MR}(t)}\right) \times 100\% \quad (8)$$

where t is a specific frame and T is the total number of frames. Table II summarizes the results. The PET template based segmentation produces regional volumes which significantly overlap the MR co-registration based segmentation volumes. Most significantly, both methods yield regional TAC and BP estimates which are largely in agreement.

The inclusion of the diffeomorphic log-demons registration following the linear registration shows a significant performance improvement in segmenting ROIs relative to the MR co-registration based method. However, there is essentially no advantage in using the non-linear registration if the task is to extract the cerebellum TAC. Since the cerebellum is a large structure, a coarse linear registration suffices for reliably extracting the cerebellum TAC. Fig. 8. shows the regional BP estimates of the left caudate using segmented regions from our PET template method compared to the MR co-registration method.

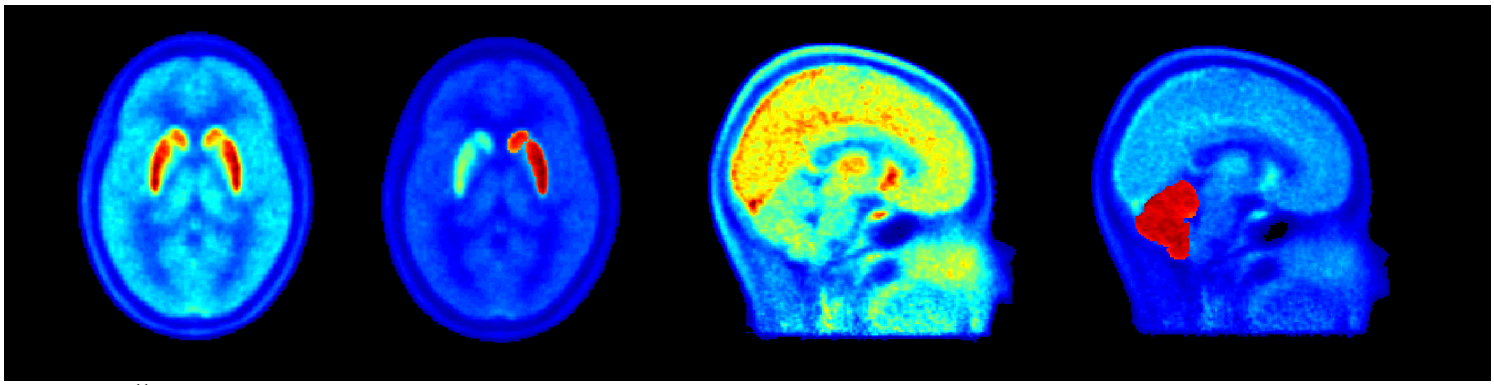

Fig. 5. Real [^{11}C]raclopride template made from 15 HRRT scans of healthy subjects. Left to right: (i) axial slice of average brain volume, (ii) axial slice labels, (iii) coronal slice of average brain volume, (iv) coronal slice labels.

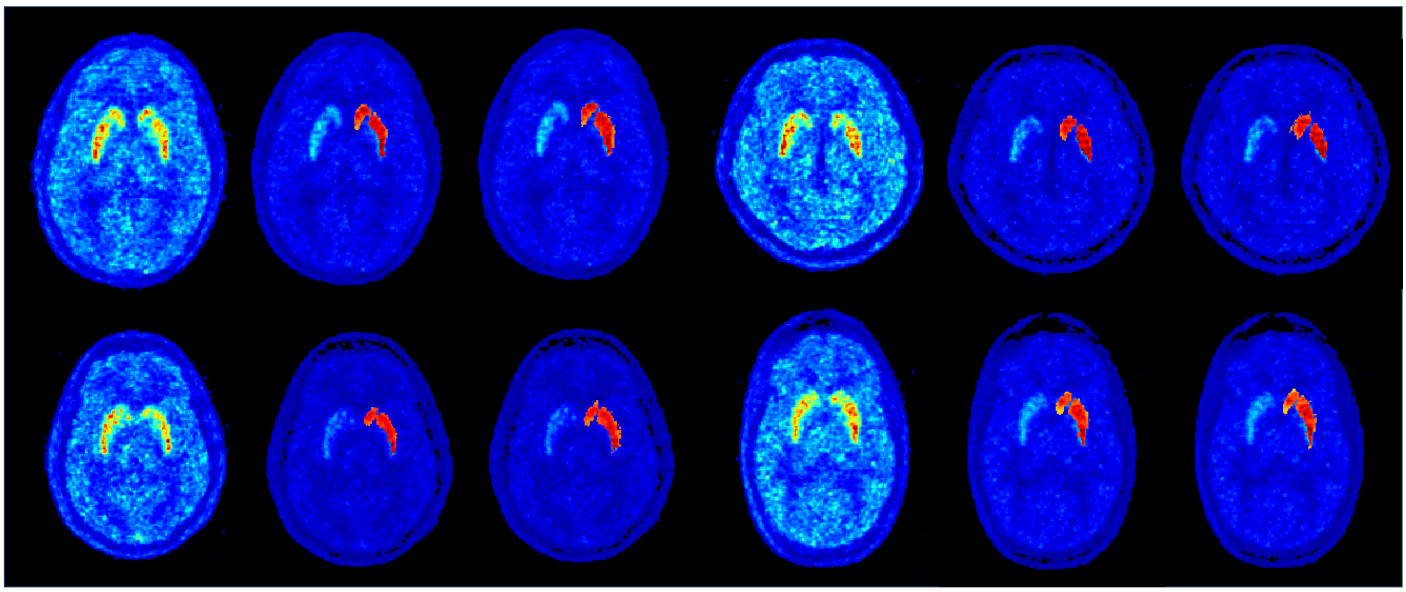

Fig. 6. Segmentation of putamen and caudate in four [^{11}C]raclopride healthy HRRT subject brain volumes. In each set of three images, the left is the original subject, the center is the PET template based segmentation results, and the right is the MR co-registration based segmentation results.

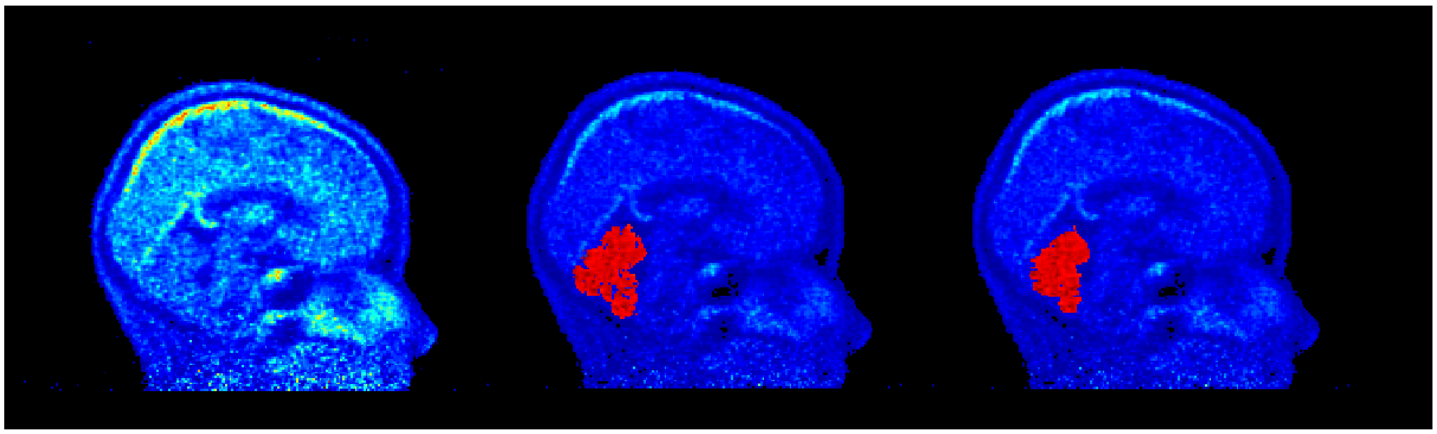

Fig. 7. Segmentation of cerebellum of a HRRT [^{11}C]raclopride scan for a healthy subject. Left to right: healthy subject, MR co-registration based segmentation, PET template based segmentation.

TABLE II: COMPARISON BETWEEN PET TEMPLATE SEGMENTATION AND THE MR CO-REGISTRATION SEGMENTATION

	$\overline{DSC}$	$\overline{\alpha_{DIFF}}$ (%)	$\overline{\kappa_{DIFF}}$ (%)
	Affine Registration Followed By DLD Registration		
Left Putamen	0.75 ± 0.05	7.5 ± 10.7	8.2 ± 4.3
Right Putamen	0.71 ± 0.06	17.1 ± 13.7	12.9 ± 5.1
Left Caudate	0.75 ± 0.04	15.1 ± 11.5	14.5 ± 5.6
Right Caudate	0.76 ± 0.04	11.3 ± 14.8	11.6 ± 6.6
Cerebellum	0.82 ± 0.11	---	1.9 ± 4.4
	Affine Registration Only		
Left Putamen	0.51 ± 0.17	-17.2 ± 25.4	-8.3 ± 15.7
Right Putamen	0.54 ± 0.13	-4.1 ± 20.7	-2.0 ± 13.4
Left Caudate	0.51 ± 0.19	-15.9 ± 26.1	-6.1 ± 14.7
Right Caudate	0.48 ± 0.18	-24.1 ± 33.0	-13.3 ± 22.1
Cerebellum	0.72 ± 0.15	---	0.5 ± 8.2

All values shown as mean plus or minus one standard deviation.

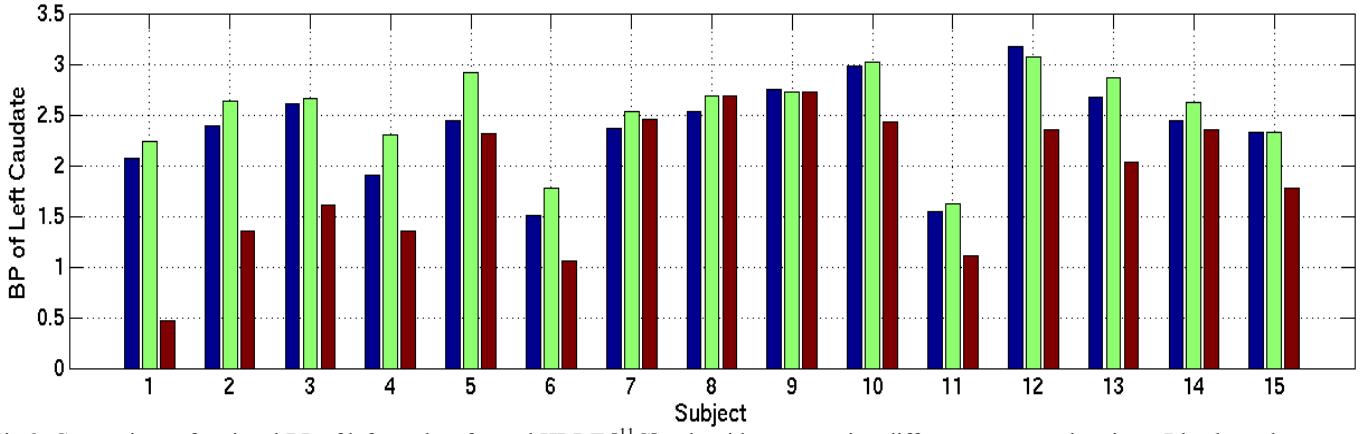

Fig 8. Comparison of regional BP of left caudate for real HRRT [^{11}C]raclopride scans using different segmented regions. Blue bars show regional BP using PET template segmented regions incorporating DLD registration. Green bars show regional BP using MR co-registration segmented regions. Red bars show results using PET template method with affine registration only.

V. Discussion

Conventional segmentation of PET images is generally performed manually by an expert on the PET image itself, or on a co-registered anatomical image. It is widely recognized that such techniques are not optimal due primarily to the time consuming nature of the process, and to the operator dependence of the ROI drawing.

Other segmentation techniques have been proposed, commonly using cluster analysis techniques [18], which classify TACs according to their shape and magnitude. However, such methods are difficult to fine-tune, and can still involve user intervention, for instance in providing locations of initial centroids needed for the algorithms.

In contrast, PET template based segmentation has been relatively unexplored. We have proposed a segmentation scheme working on static (time-summed) PET images using a high quality anatomically labeled radio-ligand specific template. The proposed scheme is completely user-independent once a manual labeling of the template is performed, enabling completely automated segmentation and regional kinetic analysis. The advantages of our proposed methodology is that it is easy to implement, and can be in general applied to images from any radio-ligand.

The methodology showed promising results using simulated data and in comparison to a traditional MR co-registration based segmentation method (CIVET). The simulated study showed that a manually labeled average image can be feasibly used to segment PET subject brain volumes and to estimate regional BP. The real data study shows that the PET template based segmentation and BP estimation compares favourably to the established standard of MR co-registration based segmentation of [^{11}C]raclopride subject brain volumes. We expect that both segmentation methods can be feasibly used to reliably identify regions of interest in subject brain volumes, and to detect relative changes in binding potential for scans of the same subject under different conditions. Using a set of [^{11}C]raclopride subject scans obtained under different experimental conditions, we will compare the performance of both segmentation methods on this basis in future work.

Bieth *et. al* [19] have developed a 4D diffeomorphic log-demons algorithm specifically for PET images, which could improve the segmentation outcome still further. However, the 4D algorithm uses a TAC-based similarity measure at the voxel level, which gives unstable registrations between noisy subject brain volumes. A pre-processing step consisting of a registration to the static template followed by a parametric fitting to denoise the voxel TACs could solve this problem, but computational time would significantly increase. This possibility will be further explored. In general, the 3D diffeomorphic log-demons registration algorithm can be optimized for PET to PET subject brain volume registration. In addition, a feature-based linear transformation prior to a non-linear transformation may improve results, since the registration outcome is highly dependent on the initialization.

In addition, in order to progress towards exploitation of fully 4D (direct) kinetic parameter estimation algorithms there is a need to perform kinetic modeling at every iterative update of the image, which ideally should not involve any user intervention.

In conclusion, our preliminary data from the simulated PET study, and comparison with conventional anatomical based segmentation, indicate that accurate tissue segmentation can be robustly achieved using our PET template method, and may replace the need for such manual or anatomically based techniques.

VI. Acknowledgments

The authors would also like to thank Dr. Alain Dagher for providing us with the [^{11}C]raclopride scans. P. Novosad acknowledges partial support by the CREATE Medical Physics Research Training Network grant of the Natural Sciences and Engineering Research Council (Grant number: 432290). This work was supported in part by NSERC (RGPIN 387067-10). This research was undertaken, in part, thanks to funding from the Canada Research Chairs program.

VII. REFERENCES

[1] H. W. de Jong, F. H. P. van Velden, R. W. Kloet, F. L. Buijs, R. Boellaard, and A. A. Lammertsma, "Performance evaluation of the ECAT HRRT: an LSO-LYSO double layer high resolution, high sensitivity scanner," *Physics in Medicine and Biology,* vol. 52, pp. 1505-1526, 2007.

[2] D. Louis Collins, C. J. Holmes, T. M. Peters, A. C. Evans, "Automatic 3-D Model-Based Neuroanatomical Segmentation," Human Brain Mapping, vol. 3, pp. 190-208, 1994.

[3] T. Vercauteren, X. Pennec, A. Perchant, and N. Ayache. "Non-parametric diffeomorphic image registration with the demons algorithm."*Medical Image Computing and Computer-Assisted Intervention - MICCAI 2007*, pp. 319-326, 2007.

[4] H. Lombaert et al., "Human Atlas of the Cardiac Fiber Architecture: Study on a Healthy Population," IEEE Transactions on Medical Imaging, vol. 31(7), pp. 1436-1447, 2012.

[5] A. Rahmim, K. Oinelle, J. Cheng, M. Shilov, W. Segars, S. Lidstone, S. Blinder, O. Rousset, H. Vajihollahi, B. Tsui et al., "Accurate event-driven motion compensation in high-resolution PET incorporating scattered and random events," *Medical Imaging, IEEE Transactions*, vol. 27, no. 8, pp. 1018-1033, 2008.

[6] J. Kim, Y. Son, H. Kim, S. Lee, S. Cho, Y. Kim, and Z. Cho, "Effects of age on dopamine 02 receptor availability in striatal subdivisions: A high-resolution positron emission tomography study," *Europeean Neuropsychopharmacology*, vol. 21, pp. 885-891, 2011.

[7] H. Hudson and R. Larkin, "Accelerated image reconstruction using ordered subsets of projection data," *Medical Imaging, IEEE Transactions on*, vol. 13, no. 4, pp. 601-609, 1994.

[8] C. Comtat, F. Bataille, C. Michel, J. Jones, M. Sibomana, L. Janeiro, and R. Trebossen, "Osem-3d reconstruction strategies for the ecat hrrt," in *Nuclear Science Symposium Conference Record*, 2004 IEEE, vol. 6. IEEE, pp. 3492-3496, 2004.

[9] A. J. Reader, P. J. Julyan, H. Williams, D. L. Hastings, and J. Zweit, "EM algorithm system modeling by image-space techniques for PET reconstruction," IEEE Transactions on Nuclear Science, vol. 50, pp. 1392-1397, Oct 2003.

[10] C. Comtat, F. C. Sureau, M. Sibomana, I. K. Hong, N. Sjoholm, and R. Trebossen, "Image based resolution modeling for the HRRT OSEM reconstructions software," *2008 IEEE Nuclear Science Symposium and Medical Imaging Conference (2008 NSS/MIC), Vols 1-9,* pp. 3395-3398, 2009.

[11] R. Gunn, A. Lammertsma, S. Hume, and V. Cunningham, "Parametric imaging of ligand-receptor binding in PET using a simplified reference region model," Neuroimage, vol. 6, pp. 279-287, 1997.

[12] Y. Ad-Dab'bagh et al., "The CIVET image-processing environment: A fully automated comprehensive pipeline for anatomical neuroimaging research", in "Proceedings of the 12th Annual Meeting of the Organization for Human Brain Mapping", M. Corbetta, ed. (Florence, Italy, NeuroImage), 2006.

[13] J.G. Sled, A.P. Zijdenbos and A.C. Evans, "A non-parametric method for automatic correction of intensity non-uniformity in MRI data", in "IEEE Transactions on Medical Imaging", vol. 17, n. 1, pp. 87-97, 1998.

[14] D. L. Collins, P. Neelin, T. M. Peters and A. C. Evans, "Automatic 3D Inter-Subject Registration of MR Volumetric Data in Standardized Talairach Space," Journal of Computer Assisted Tomography, 18(2) pp. 192-205, 1994.

[15] J. Mazziotta, A. Toga, A. Evans, P. Fox, J. Lancaster, K. Zilles, R. Woods, T. Paus, G. Simpson, B. Pike, C. Holmes, L. Collins, P. Thompson, D. MacDonald, M. Iacoboni, T. Schormann, K. Amunts, N. Palomero-Gallagher, S. Geyer, L. Parsons, K. Narr, N. Kabani, G. Le Goualher, D. Boomsma, T. Cannon, R. Kawashima, and B. Mazoyer, "A probabilistic atlas and reference system for the human brain: International Consortium for Brain Mapping (ICBM)," Philos Trans R Soc Lond B Biol Sci, vol. 356, pp. 1293-322, 2001.

[16] S.M. Smith, "Fast robust automated brain extraction," Human Brain Mapping, 17(3):143-155, November 2002.

[17] Zijdenbos, A., Forghani, R., and Evans, A., "Automatic Quantification of MS Lesions in 3D MRI Brain Data Sets: Validation of INSECT,". In Medical Image Computing and Computer-Assisted Intervention (MICCAI98), W.M. Wells, A. Colchester, and S. Delp, eds. (Cambridge, MA, Springer-Verlag Berlin Heidelberg), pp. 439-448, 1998.

[18] K.P. Wong, F. Deng, S.R. Meikle and M.J. Fulham,"Segmentation of Dynamic PET Images Using Cluster Analysis," IEEE Transactions on Nuclear Science, vol. 49, no.1, pp. 200-207, 2002.

[19] M. Bieth, H. Lombaert, A.J. Reader, K. Siddiqi, "Atlas Construction for Dynamic (4D) PET Using Diffeomorphic Transformations," Medical Image Computing and Computer-Assisted Intervention – MICCAI 2013, Lecture Notes in Computer Science Volume 8150, pp 35-42, 2013.